Computers and Geotechnics 87 (2017) 149–162

Contents lists available at ScienceDirect

Computers and Geotechnics

journal homepage: www.elsevier.com/locate/compgeo

Research Paper

Uncertainty of rainfall-induced landslides considering spatial variability of parameters

Jing-Sen Cai [a,c], Tian-Chyi Jim Yeh [b,c,*], E-Chuan Yan [a], Yong-Hong Hao [b], Shao-Yang Huang [d], Jet-Chau Wen [e]

[a] Faculty of Engineering, China University of Geosciences, Wuhan 430074, China
[b] Tianjin Key Laboratory of Water Resources and Environment, Tianjin Normal University, Tianjin, China
[c] Department of Hydrology and Water Resources, University of Arizona, Tucson, AZ 85721, USA
[d] Graduate School of Engineering Science and Technology, National Yunlin University of Science and Technology, Douliou, Taiwan
[e] Research Center for Soil and Water Resources and Natural Disaster Prevention, National Yunlin University of Science and Technology, Douliu, Taiwan

ARTICLE INFO

Article history:
Received 16 November 2016
Received in revised form 5 January 2017
Accepted 10 February 2017

Keywords:
Rainfall infiltration
Slope stability uncertainty
Cross correlation
Spatial variability
Hydraulic conductivity
Shear strength

ABSTRACT

A cross-correlation analysis is conducted to determine the impacts of the heterogeneity of hydraulic conductivity K_s, soil cohesion c' and soil friction angle (tan φ') on the uncertainty of slope stability in time and space during rainfall. We find the relative importance of tan φ' and c' depends on the effective stress. While the sensitivity of the stability to the variability of K_s is small, the large coefficient of variation of K_s may exacerbate the variability of pore-water pressure. Therefore, characterizing the heterogeneity of hydraulic properties and pore-water distribution in the field is critical to the stability analysis.

1. Introduction

Properties of geologic formation generally exhibit a high degree of spatial variabilities at a multiplicity of scales. It is practically impossible to characterize them in detail within a slope. This reality forces us to cope with uncertain in our evaluations of slope stability. Slope stability analysis considering spatial variability of soil properties thus has become popular in recent years (e.g., [3,5,7–10,14–18,21,29,30,32,36]). The soil properties, which are considered significant to the slope stability and commonly discussed in literatures, are the shear strength parameters (the effective cohesion c' and the effective soil friction angle ϕ') and the saturated hydraulic conductivity K_s.

Previous studies show that the spatial variability of the shear strength parameters has various effects on the slope stability under different circumstances. For infinite slopes, studies [3,16] showed that analyses without properly accounting for spatial variability can lead to unconservative estimates of the probability of slope failure. Li et al. [22] emphasized that the probability of slope failure will be overestimated if a linear increasing trend underlying the shear strength parameter is ignored or simplified as a constant. For two-dimensional slopes, Ji et al. [18] found that ignoring spatial variability of the shear strength parameters significantly overestimated the failure probability. Cho [9] stressed the importance of spatial variability of soil properties with regard to the outcome of a probability assessment. Griffiths et al. [15] and Jiang et al. [20] pointed out that ignoring spatial variability of shear strength parameters could lead to non-conservative estimates (underestimation) of the probability of slope failure, when the coefficients of variation of the shear strength parameters are large, and the factor of safety evaluated at mean parameters is close to 1.

The effect of spatial variability of the saturated hydraulic conductivity K_s on the slope stability is complex. Santoso et al. [29] pointed out that considering spatial variability of K_s, their analysis can lead to a shallow slope failure, which does not exist in the analysis using a homogeneous slope. As mentioned by Cho [7], in the early stage of infiltration, the wetting front's advancement decreases the factor of safety at the slope's upper portion, and hence, the critical failure surface likely exists in the upper portion of the slope. As infiltration progresses, the critical failure surface moves downwards, and the likelihood of failure at the base of the slope continuously decreases. Besides, at early time, a large

* Corresponding author at: Tianjin Key Laboratory of Water Resources and Environment, Tianjin University, 393 Binshuixidao Road, Xiqing District, Tianjin 300387, China and Department of Hydrology and Water Resources, The University of Arizona, 1133 E. James E. Rogers Way, 122 Harshbarger Bldg 11, Tucson, AZ 85721, USA.

E-mail addresses: cjs619242601@gmail.com (J.-S. Cai), yeh@hwr.arizona.edu (T.-C.J Yeh).

http://dx.doi.org/10.1016/j.compgeo.2017.02.009
0266-352X/

vertical correlation scale or a small coefficient of variation of K_s lead to a small probability of failure at the impermeable slope base. On the contrary, a large vertical correlation scale or a large coefficient of variation of K_s may yield a large probability of the failure at the base at late time.

Previous studies have focus on the effects of mean, variance, and correlation structure (i.e., the averaged thickness, width, and length of the heterogeneity) of parameters on the probability of slope failure. That is, these works reveal influences of the uncertainty or spatial variability of properties over the entire slope, without resorting to the detailed spatial distributions of properties. On the other hand, the temporal evolution of the role of uncertainties of different properties (such as K_s and c', ϕ') at different locations in the slope stability and the spatial relationship between the stability of a potential slip surface and heterogeneity at various parts of a slope remain relatively unexplored. Rainfall infiltration processes in slopes are generally complex because of the presence of saturated and unsaturated zones and the time-varying water table, in addition to the heterogeneous nature of geologic media. The effect of heterogeneity of different properties on the slope stability would evolve with time during rainfall infiltration processes, and deserves further investigation. In addition, the effects of spatial variabilities of hydraulic properties (e.g., K_s) and mechanical properties (e.g., c', ϕ') on slope stability are generally investigated separately, and their relative importance to uncertainties of slope stability and their interaction are poorly understood. Furthermore, all these previous studies have relied on Monte Carlo (MC) simulation, which is often dependent on generated realizations of parameter values. Using such an approach, it is also difficult to examine the direct relationship between these properties and slope stability.

The objective of this study is to provide a better understanding of the temporal and spatial evolution of uncertainty of slope stability during rainfall, considering uncertainty or spatial variability of parameters. In order to achieve this objective, we first investigate the temporal and spatial evolution of cross correlations between the factor of safety at a potential slip surface and the saturated hydraulic conductivity and the shear strength parameters during a rainfall infiltration process in homogeneous and heterogeneous infinite slopes. Subsequently, the contributions to the standard deviation of FS_i at a potential slip surface from the variation of each parameter are presented, using the typical ranges of the variation of parameters reported in literature. Finally, seepage and stability analyses of two typical heterogeneous slopes are used to illustrate how the heterogeneities of soil properties influence the slope stability, and to demonstrate the importance of the cross-correlation analysis of heterogeneous slope on the stability analysis of heterogeneous slope under rainfall infiltration.

2. Methodology

2.1. Basic equations

The factor of safety along ith potential slip surface (i.e., FS_i) of an infinite slope can be evaluated using the limit equilibrium model (LEM) with a unified effective stress under both saturated and unsaturated conditions [23]. If we let the pore air pressure u_a be atmospheric pressure (i.e., $u_a = 0$), FS_i can be expressed as (e.g., [1,7,16,22]):

$$FS_i = \frac{((H-z_i)\gamma_i \cos^2\beta - \sigma_i^s)\tan\phi_i' + c_i'}{(H-z_i)\gamma_i \sin\beta\cos\beta} = \left(\frac{1}{\tan\beta} + \frac{-\sigma_i^s}{(H-z_i)\gamma_i \sin\beta\cos\beta}\right)\tan\phi_i' + \frac{c_i'}{(H-z_i)\gamma_i \sin\beta\cos\beta} \quad (0 \leqslant z_i < H,\ i = 1,\ldots,n) \tag{1}$$

where β is the slope inclination; γ_i is the averaged total unit weight above ith potential slip surface; H denotes the vertical distance of soils from the slope base to the land surface; c_i' and ϕ_i' are the effective cohesion and the effective soil friction angle at ith potential slip surface, and z_i is the elevation (positive upward) of ith potential slip surface relative to the slope base (see Fig. 1); σ_i^s represents the effective negative pore water pressure under unsaturated conditions or effective positive pore water pressure under saturated conditions at ith potential slip surface [23].

The factor of safety for the entire slope (denoted as FS) is:

$$FS = \min\{FS_i\} = \min\left\{\left(\frac{1}{\tan\beta} + \frac{-\sigma_i^s}{(H-z_i)\gamma_i \sin\beta\cos\beta}\right)\tan\phi_i' + \frac{c_i'}{(H-z_i)\gamma_i \sin\beta\cos\beta}\right\} \quad (0 \leqslant z_i < H,\ i = 1,\cdots,n) \tag{2}$$

According to [23], σ_i^s can be expressed as:

$$\sigma_i^s = -\frac{\theta_i - \theta_r}{\theta_s - \theta_r}(u_a - u_{w_i}) = -S_{e_i}(u_a - u_{w_i}) \tag{3}$$

where u_{wi}, S_{e_i} and θ_i are the pore water pressure, the effective water saturation and the volumetric moisture content at ith potential slip surface, respectively; θ_s and θ_r denote the saturated and residual volumetric moisture contents, respectively. $\sigma_i^s = S_{e_i}u_{w_i} < 0$ for unsaturated conditions ($u_{w_i} < 0$), $\sigma_i^s = u_{w_i} \geqslant 0$ for saturated conditions ($u_{w_i} \geqslant 0$). Via this unified effective stress theory, Eq. (1) can account for both the reduction in matric suction and the development of positive pore water pressure in a continuous form [7,23].

In this paper, the variation in unit weight resulting from changes in moisture content during infiltration is considered by integration of the moisture content profile above the potential slip surface. That is, the total unit weight γ_i can be expressed as follows:

$$\gamma_i = \frac{1}{H-z_i}\int_{z_i}^{H}(\gamma_d + \theta(z)\gamma_w)dz \quad (0 \leqslant z_i < H) \tag{4}$$

where γ_d is the dry unit weight of the soil; γ_w is the unit weight of water.

The rainfall infiltration process in the infinite slope is assumed described by a one-dimensional governing vertical flow equation:

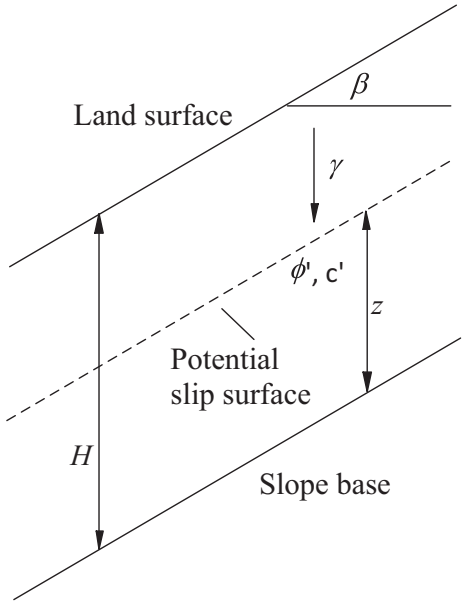

Fig. 1. An infinite slope model.

$$\frac{\partial}{\partial z}\left(K(h)\left(\frac{\partial h}{\partial z}+1\right)\right)=[\eta S_s+C(h)]\frac{\partial h}{\partial t} \tag{5}$$

where z denotes the coordinate along vertical z-axis (positive upward); h is the pressure head; $K(h)$ is the hydraulic conductivity; S_s is the specific storage; $C(h)$ denotes the moisture capacity term; t denotes time; η is the saturation index. h is a positive value if the medium is fully saturated and is negative if the medium is unsaturated. The relationship between u_w and h is $u_w = h\gamma_w$. $K(h)$ varies with pressure head under unsaturated conditions. S_s represents the percentage of water released from a unit volume of fully saturated porous media under a unit decline in hydraulic head. On the other hand, $C(h)=\frac{\partial\theta}{\partial h}\big|_h$ is the change in moisture content in a unit volume of the porous medium under a unit change of negative pressure head, when the medium is under unsaturated conditions. In other words, it is the gradient of moisture-pressure constitutive relationship (i.e. moisture retention curve) at a given pressure head. While S_s and $C(h)$ are similar in definition, the physical mechanisms they represented are quite different. S_s is related to the compressibility of porous media and water while the medium remains fully saturated, whereas $C(h)$ represents desaturation or saturation of the pores in the medium. On the right-hand side of Eq. (5), η is set to 1 if the medium is saturated and 0 if the medium is unsaturated.

The hydraulic conductivity-pressure head and moisture-pressure head constitutive relationships of the soil within the slope are assumed to be described by an exponential model [12]:

$$K(h)=K_s\exp(\alpha h) \tag{6a}$$

$$\theta(h)=\theta_r+(\theta_s-\theta_r)\exp(\alpha h) \tag{6b}$$

, respectively, where α is the pore size distribution parameter.

2.2. Cross-correlation analysis

This section describes the cross-correlation analyses for slope stability during rainfall infiltration process in homogeneous and heterogeneous slopes. Table 1 summarizes the statistics of the soil properties used for the analysis.

2.2.1. Homogeneous slope

In homogeneous slope cases, the parameters, K_s, c' and $\tan\phi'$ values of the slope are uniform in space but they are uncertain due to either measurement errors or lack of measurements. A probabilistic approach is thus used to analyze the uncertainty in the analysis of FS_i in a slope during rainfall infiltration. This approach assumes that each parameter (such as K_s, c' and $\tan\phi'$) is a random variable although it is spatially uniform. Because of the uncertainty of each parameter, we express $K_s=\mu_{K_s}+p_{K_s}$, $c'=\mu_{c'}+p_{c'}$ and $\tan\phi'=\mu_{\tan\phi'}+p_{\tan\phi'}$, where μ_{K_s}, $\mu_{c'}$ and $\mu_{\tan\phi'}$ are their means (the most likely values) and p_{K_s}, $p_{c'}$ and $p_{\tan\phi'}$ denote their perturbations (deviations from the means). Likewise, the uncertainty in the FS_i is represented by $FS_i=\mu_{FS_i}+p_{FS_i}$, where μ_{FS_i} is the mean and p_{FS_i} is the perturbation. Expanding the FS_i in Eq. (1) in a Taylor series about the mean values of parameters, and neglecting second-order and higher order terms (in fact, only the relationship between FS_i and K_s is nonlinear and first-order approximation is applied), the FS_i at ith potential slip surface at a given time t can be expressed as:

$$FS(z_i,t)=\mu_{FS}(z_i,t)+p_{FS}(z_i,t)=\mu_{FS}(z_i,t)+\left.\frac{\partial FS(z_i,t)}{\partial K_s}\right|_{\mu}p_{K_s}+\left.\frac{\partial FS(z_i,t)}{\partial c'}\right|_{\mu}p_{c'}+\left.\frac{\partial FS(z_i,t)}{\partial\tan\phi'}\right|_{\mu}p_{\tan\phi'}\ (i=1,\ldots,n) \tag{7}$$

where the derivative is the Jacobian, the sensitivity of $FS(z_i,t)$ to the change of a given parameter. The vertical bar with subscript μ implies that the sensitivity is evaluated at the mean values of all parameters. After subtracting the mean part in Eq. (7), the FS_i perturbation is

$$p_{FS}(z_i,t)=J_{FSK_s}(z_i,t)p_{K_s}+J_{FSc'}(z_i,t)p_{c'}+J_{FS\tan\phi'}(z_i,t)p_{\tan\phi'}\ (i=1,\ldots,n) \tag{8}$$

in which J is the Jacobian.

Assuming that the perturbations of the different parameters are mutually independent from each other, multiplying Eq. (8) by itself on both sides, and taking the expected value of the result lead to:

$$\sigma^2_{FS}(z_i,t)=\left(J_{FSK_s}(z_i,t)\right)^2\sigma^2_{K_s}+\left(J_{FSc'}(z_i,t)\right)^2\sigma^2_{c'}+\left(J_{FS\tan\phi'}(z_i,t)\right)^2\sigma^2_{\tan\phi'}\ (i=1,\ldots,n) \tag{9}$$

where $\sigma^2_{FS}(z_i,t)$ is the FS_i variance at (z_i,t); $\sigma^2_{K_s}$, $\sigma^2_{c'}$ and $\sigma^2_{\tan\phi'}$ are the variance of K_s, c' and $\tan\phi'$, respectively. $\sigma^2_{FS}(z_i,t)$ represents possible deviation of the evaluated FS_i from μ_{FS_i} at a given (z_i,t). Here, the different parameters are assumed independent from each other since their cross covariances are generally unknown.

Based on Eq. (8), the cross-covariance between FS_i and a parameter can be derived by multiplying the parameter perturbation on both sides of the equation and taking the expected value of the resultant equation. That is,

$$\sigma^2_{FSK_s}(z_i,t)=J_{FSK_s}(z_i,t)\sigma^2_{K_s}\ (i=1,\ldots,n) \tag{10a}$$

$$\sigma^2_{FSc'}(z_i,t)=J_{FSc'}(z_i,t)\sigma^2_{c'}\ (i=1,\ldots,n) \tag{10b}$$

$$\sigma^2_{FS\tan\phi'}(z_i,t)=J_{FS\tan\phi'}(z_i,t)\sigma^2_{\tan\phi'}\ (i=1,\ldots,n) \tag{10c}$$

where $\sigma^2_{FSK_s}(z_i,t)$, $\sigma^2_{FSc'}(z_i,t)$ and $\sigma^2_{FS\tan\phi'}(z_i,t)$ are the cross-covariance between FS_i and K_s, c', $\tan\phi'$, respectively. These cross-covariances can be normalized by the square root of the product of $\sigma^2_{FS}(z_i,t)$ and the corresponding parameter variance to derive their cross-correlation functions. The cross correlation, denoted as ρ, between the FS_i at (z_i,t) and K_s, c', $\tan\phi'$ are

$$\rho_{FSK_s}(z_i,t)=\frac{J_{FSK_s}(z_i,t)\sigma^2_{K_s}}{\sqrt{\sigma^2_{FS}(z_i,t)\sigma^2_{K_s}}}=\frac{J_{FSK_s}(z_i,t)\sigma_{K_s}}{\sigma_{FS}(z_i,t)}(i=1,\ldots,n) \tag{11a}$$

$$\rho_{FSc'}(z_i,t)=\frac{J_{FSc'}(z_i,t)\sigma^2_{c'}}{\sqrt{\sigma^2_{FS}(z_i,t)\sigma^2_{c'}}}=\frac{J_{FSc'}(z_i,t)\sigma_{c'}}{\sigma_{FS}(z_i,t)}\ (i=1,\ldots,n) \tag{11b}$$

$$\rho_{FS\tan\phi'}(z_i,t)=\frac{J_{FS\tan\phi'}(z_i,t)\sigma^2_{\tan\phi'}}{\sqrt{\sigma^2_{FS}(z_i,t)\sigma^2_{\tan\phi'}}}=\frac{J_{FS\tan\phi'}(z_i,t)\sigma_{\tan\phi'}}{\sigma_{FS}(z_i,t)}\ (i=1,\ldots,n) \tag{11c}$$

Table 1
Prior statistics of K_s, c' and $\tan\phi'$, related parameters and slope geometrical parameters.

Parameters	Values
Mean of K_s, μ_{K_s}	0.2592 m/d
Mean of c', $\mu_{c'}$	5.0 kN/m^2
Mean of ϕ', $\mu_{\phi'}$	32°
COVs of K_s, c' and $\tan\phi'$	1, lower bound, upper bound
Correlation scale, λ	0.3 m, 0.8 m
Specific storage, S_s	0.001 m^{-1}
Saturated volumetric moisture content, θ_s	0.358
Residual volumetric moisture content, θ_r	3.58×10^{-4}
Coefficient in exponential model, α	0.5 m^{-1}
Slope height, H	2 m
Slope angle, β	40°
Dry unit weight, γ_d	16 kN/m^3
Unit weight of water, γ_w	9.8 kN/m^3

, respectively. Note that these cross correlations are dimensionless (ranging from −1 to +1) and represent the relationship between the uncertainty of a given parameter of the homogeneous slope and the uncertainty in the stability of a potential slip surface at a given time due to uncertainty of all parameters.

2.2.2. Heterogeneous slope

In order to investigate the effect of parameter heterogeneity on the slope stability, we assume that each parameter (such as $K_s(z_i)$, $c'(z_i)$ or $\tan\phi'(z_i)$, $i = 1,\ldots,n$) of the slope is a spatial random field or stochastic process. That is to say, the slope has a random variable (e.g., K_s) at each location, which has a mean value and a variance, representing the uncertainty due to the spatial variability as well as lack of measurements. The slope thus is made of many these random variables. This collection of random variables is called a stochastic process or random field, which is characterized by a joint probability distribution (see [33]). Consequently, these parameters are expressed in terms of their means and perturbations:

$$K_s(z_i) = \mu_{K_s} + p_{K_s}(z_i)\ (i = 1,\ldots,n) \tag{12a}$$

$$c'(z_i) = \mu_{c'} + p_{c'}(z_i)\ (i = 1,\ldots,n) \tag{12b}$$

$$\tan\phi'(z_i) = \mu_{\tan\phi'} + p_{\tan\phi'}(z_i)\ (i = 1,\ldots,n) \tag{12c}$$

Similarly, the FS_i perturbation at ith potential slip surface at a given time t can be approximated as:

$$p_{FS}(z_i,t) = \sum_{j=1}^{n}\left.\frac{\partial FS(z_i,t)}{\partial K_s(z_j)}\right|_{\mu} p_{K_s}(z_j) + \sum_{j=1}^{n}\left.\frac{\partial FS(z_i,t)}{\partial c'(z_j)}\right|_{\mu} p_{c'}(z_j) + \sum_{j=1}^{n}\left.\frac{\partial FS(z_i,t)}{\partial \tan\phi'(z_j)}\right|_{\mu} p_{\tan\phi'}(z_j)\ (i,j = 1,\ldots,n) \tag{13}$$

The derivatives (i.e., sensitivities) in Eq. (13) represent the change in FS_i at ith potential slip surface at time t due to unit change in the parameter at location z_j in the domain. Eq. (13) can also be written in a matrix form:

$$\mathbf{p}_{FS}(t) = \mathbf{J}_{FSK_s}(t)\mathbf{p}_{K_s} + \mathbf{J}_{FSc'}(t)\mathbf{p}_{c'} + \mathbf{J}_{FS\tan\phi'}(t)\mathbf{p}_{\tan\phi'} \tag{14}$$

where $\mathbf{p}_{FS}$, $\mathbf{p}_{K_s}$, $\mathbf{p}_{c'}$ and $\mathbf{p}_{\tan\phi'}$ are $n\times 1$ vectors. $\mathbf{J}_{FSK_s}$, $\mathbf{J}_{FSc'}$ and $\mathbf{J}_{FS\tan\phi'}$ are $n\times n$ Jacobian matrices. Assuming that different parameters are mutually independent of each other, the cross-covariance matrices between FS_i at (z_i,t) and different given parameters at z_j in the slope become

$$\mathbf{R}_{FSK_s}(t) = \mathbf{J}_{FSK_s}(t)\mathbf{R}_{K_sK_s} \tag{15a}$$

$$\mathbf{R}_{FSc'}(t) = \mathbf{J}_{FSc'}(t)\mathbf{R}_{c'c'} \tag{15b}$$

$$\mathbf{R}_{FS\tan\phi'}(t) = \mathbf{J}_{FS\tan\phi'}(t)\mathbf{R}_{\tan\phi'\tan\phi'} \tag{15c}$$

where $\mathbf{R}_{FSK_s}$, $\mathbf{R}_{FSc'}$, $\mathbf{R}_{FS\tan\phi'}$ are $n\times n$ cross-covariance matrices for K_s, c' and $\tan\phi'$, respectively; $\mathbf{R}_{K_sK_s}$, $\mathbf{R}_{c'c'}$, $\mathbf{R}_{\tan\phi'\tan\phi'}$ are $n\times n$ auto-covariance matrices for K_s, c' and $\tan\phi'$, respectively. Each auto-covariance matrix represents the spatial statistical relationships between a parameter (e.g., K_s) at a given location and the parameter at a different location. The spatial relationships of K_s, c' and $\tan\phi'$ are modeled with an exponential function (e.g., [5]) with the same correlation scale λ in z direction. Spatial correlation scale λ represents the distance within which the soil properties (such as K_s, c' or $\tan\phi'$) are correlated in space. Physically, it describes the average thickness of layers or stratifications in this slope [33]. The corresponding FS_i auto-covariance matrix $\mathbf{R}_{FSFS}$ based on Eq. (14) is given as

$$\mathbf{R}_{FSFS}(t) = \mathbf{J}_{FSK_s}(t)\mathbf{R}_{K_sK_s}\mathbf{J}^T_{FSK_s}(t) + \mathbf{J}_{FSc'}(t)\mathbf{R}_{c'c'}\mathbf{J}^T_{FSc'}(t) + \mathbf{J}_{FS\tan\phi'}(t)\mathbf{R}_{\tan\phi'\tan\phi'}\mathbf{J}^T_{FS\tan\phi'}(t) \tag{16}$$

where the superscript T denotes the transpose. The diagonal components of $\mathbf{R}_{FSFS}$ are the FS_i variances ($i = 1,\ldots,n$) at time t, which are denoted as $\sigma^2_{FS}(z_i,t)$ ($i = 1,\ldots,n$). The $\sigma^2_{FS}(z_i,t)$ represents the uncertainty in FS_i at ith potential slip surface at time t, due to uncertainty in parameters at different locations over the entire domain.

The cross-correlation matrices, denoted as $\boldsymbol{\rho}$, between FS_i at (z_i,t) and K_s, c', $\tan\phi'$ at z_j can be obtained by normalizing the cross-covariances in Eq. (15) with the square root of the product of the variance of FS_i at (z_i,t) and the corresponding variance of the parameter:

$$\boldsymbol{\rho}_{FSK_s}(t) = \frac{\mathbf{R}_{FSK_s}(t)}{\sqrt{\sigma^2_{FS}(z_i,t)\sigma^2_{K_s}}} = \frac{\mathbf{J}_{FSK_s}(t)\mathbf{R}_{K_sK_s}}{\sqrt{\sigma^2_{FS}(z_i,t)\sigma^2_{K_s}}}\ (i = 1,\ldots,n) \tag{17a}$$

$$\boldsymbol{\rho}_{FSc'}(t) = \frac{\mathbf{R}_{FSc'}(t)}{\sqrt{\sigma^2_{FS}(z_i,t)\sigma^2_{c'}}} = \frac{\mathbf{J}_{FSc'}(t)\mathbf{R}_{c'c'}}{\sqrt{\sigma^2_{FS}(z_i,t)\sigma^2_{c'}}}\ (i = 1,\ldots,n) \tag{17b}$$

$$\boldsymbol{\rho}_{FS\tan\phi'}(t) = \frac{\mathbf{R}_{FS\tan\phi'}(t)}{\sqrt{\sigma^2_{FS}(z_i,t)\sigma^2_{\tan\phi'}}} = \frac{\mathbf{J}_{FS\tan\phi'}(t)\mathbf{R}_{\tan\phi'\tan\phi'}}{\sqrt{\sigma^2_{FS}(z_i,t)\sigma^2_{\tan\phi'}}}\ (i = 1,\ldots,n) \tag{17c}$$

These cross correlations are not only the sensitivities of FS_i to changes in different parameters, they also consider the possible magnitude of heterogeneity (variance) of parameters, and the spatial correlation of parameters which reflects the spatial structure of heterogeneity. As discussed in Mao et al. [25] and Sun et al. [31], the cross-correlation analysis is the sensitivity analysis cast in a stochastic framework with the consideration of possible spatial relationship between parameters at different locations.

2.3. Sensitivity analysis

In this section, we formulate the sensitivity of the FS_i with respect to every parameter, which is required in the evaluation of cross correlations.

There exist analytical solutions for calculating the sensitivity of the FS_i with respect to c' and $\tan\phi'$. For homogeneous slopes:

$$J_{FS_ic'}(t) = \left.\frac{\partial FS(z_i,t)}{\partial c'}\right|_{\mu} = \frac{1}{(H-z_i)\mu_{\gamma_i}(t)\sin\beta\cos\beta}\quad (0\leqslant z_i < H,\ i = 1,\ldots,n) \tag{18a}$$

$$J_{FS_i\tan\phi'}(t) = \left.\frac{\partial FS(z_i,t)}{\partial \tan\phi'}\right|_{\mu} = \frac{1}{\tan\beta} + \frac{-\mu_{\sigma^s_i}(t)}{(H-z_i)\mu_{\gamma_i}(t)\sin\beta\cos\beta}\quad (0\leqslant z_i < H, i = 1,\ldots,n) \tag{19a}$$

where $\mu_{\gamma_i}(t)$ and $\mu_{\sigma^s_i}(t)$ denote the mean value of γ_i and σ^s_i at time t, respectively.

For heterogeneous slopes:

$$J_{FS_ic'_j}(t) = \left.\frac{\partial FS(z_i,t)}{\partial c'(z_j)}\right|_{\mu} = \begin{cases} \dfrac{1}{(H-z_i)\mu_{\gamma_i}(t)\sin\beta\cos\beta} & i = j \\ 0 & i\neq j \end{cases}\quad (0\leqslant z_i < H, i,j = 1,\ldots,n) \tag{18b}$$

$$J_{FS_i\tan\phi'_j}(t) = \left.\frac{\partial FS(z_i,t)}{\partial \tan\phi'(z_j)}\right|_{\mu} = \begin{cases} \dfrac{1}{\tan\beta} + \dfrac{-\mu_{\sigma^s_i}(t)}{(H-z_i)\mu_{\gamma_i}(t)\sin\beta\cos\beta} & i = j \\ 0 & i\neq j \end{cases}\quad (0\leqslant z_i < H, i,j = 1,\ldots,n) \tag{19b}$$

That is, $\mathbf{J}_{FSc'}$ and $\mathbf{J}_{FS\tan\phi'}$ are $n\times n$ diagonal matrices.

However, due to the nonlinearity, the sensitivity of the FS_i with respect to K_s needs to be evaluated numerically. In this study, a

perturbation approach is employed. For homogeneous slopes, it solves Eq. (1) for FS_i, using μ_{K_s} and a perturbed value $\mu_{K_s} + \Delta K_s$. Then, a first-order numerical approximation of $J_{FS_iK_s}$ is given as

$$J_{FS_iK_s}(t) = \left.\frac{\partial FS(z_i,t)}{\partial K_s}\right|_{\mu} = \left.\frac{\Delta FS(z_i,t)}{\Delta K_s}\right|_{\mu} = \frac{FS|_{\mu_{K_s}+\Delta K_s}(z_i,t) - FS|_{\mu_{K_s}}(z_i,t)}{\Delta K_s} \quad (i = 1,\ldots,n) \tag{20a}$$

For heterogeneous slopes, it solves Eq. (1) for FS_i, using μ_{K_s} and a perturbed value $\mu_{K_s} + \Delta K_{sj}$. Then, a first-order numerical approximation of $J_{FS_iK_{sj}}$ is given as

$$J_{FS_iK_{sj}}(t) = \left.\frac{\partial FS(z_i,t)}{\partial K_s(z_j)}\right|_{\mu} = \left.\frac{\Delta FS(z_i,t)}{\Delta K_s(z_j)}\right|_{\mu} = \frac{FS|_{\mu_{K_s}+\Delta K_{sj}}(z_i,t) - FS|_{\mu_{K_s}}(z_i,t)}{\Delta K_s(z_j)} \quad (i,j = 1,\ldots,n) \tag{20b}$$

2.4. Numerical experiments

A shallow layered slope above a bedrock is used to demonstrate the cross-correlation analysis. The geometrical parameters and all the hydraulic and mechanical parameters used in this paper are listed in Table 1. These parameter values are mainly based on those used in the study by Cho [7]. According to Cho [7], the type of soil used here is a typical weathered granite soil, sampled in Seochang, Korea.

Also following Cho [7], the initial pressure head distribution in the slope is −2 m through the depth with the impermeable boundary located at the slope base. As rainfall occurs, a constant zero pressure head is assigned to the top boundary to represent a constant rainfall intensity.

This study employs a two-dimensional finite element analysis code [35] to simulate the one-dimensional vertical seepage described by Eq. (5). Subsequently, computed vertical profiles of pore water pressure, effective water saturation and moisture content from transient finite element seepage analyses are used as inputs for calculating FS_i $(i = 1,\ldots,n)$ at each time step by Eq. (1). The entire infinite slope is discretized into 40 elements in the vertical direction. That is, 40 potential slip surfaces (i.e., $n = 40$) of different depths at an interval (Δz) of 0.05 m are considered; each element has a width of 1 m. These potential slip surfaces are numbered 1–40 from slope base to land surface (see Fig. 1).

3. Results and discussions

The results and discussions will be grouped into (1) deterministic analysis using the mean value of soil properties, (2) homogeneous slope model considering the uncertainty of soil properties, and (3) heterogeneous slope model considering the spatial variability of soil properties. All these three groups are with the same configurations of the slope geometry, grid mesh (elements), initial and boundary conditions. The values of the parameters used are kept the same unless specified.

3.1. Deterministic analysis

First, a deterministic transient seepage analysis is conducted, by using the mean values of the soil properties (i.e., μ_{K_s}, $\mu_{c'}$, $\mu_{\tan\phi'}$), to study rainfall infiltration into the infinite slope with the impermeable boundary located at the slope base. The vertical profiles of simulated pore water pressure and the corresponding factor of safety at five different times (0.001, 0.03, 0.1, 0.5, 1 day) are displayed in Fig. 2a and b, respectively. As shown in Fig. 2a, the matrix suction vanishes near the land surface after a short duration of rainfall. We define the wetting front as the location where the pressure changes from the initial pressure to the less negative pressure (even the positive pressure) induced by the infiltrating water. The wetting front propagates as rainfall infiltration continues until it reaches the slope base. The wetting profiles are relatively gentle without a drastic change in moisture content at the front due to the hydraulic conductivity-pressure head and moisture-pressure head constitutive relationships of the soil. The matrix suction of the soil behind the wetting front zone gradually reduces over time and the soil becomes saturated afterwards. If the rainfall continues when the wetting front zone reaches the impermeable slope base, positive pore water pressure builds up and the phreatic surface in the slope rises, finally (after 1 day) the flow becomes statics and fully saturated within the entire slope. Fig. 2b shows the effect of infiltration on slope stability. The wetting front's advancement due to rainfall infiltration decreases

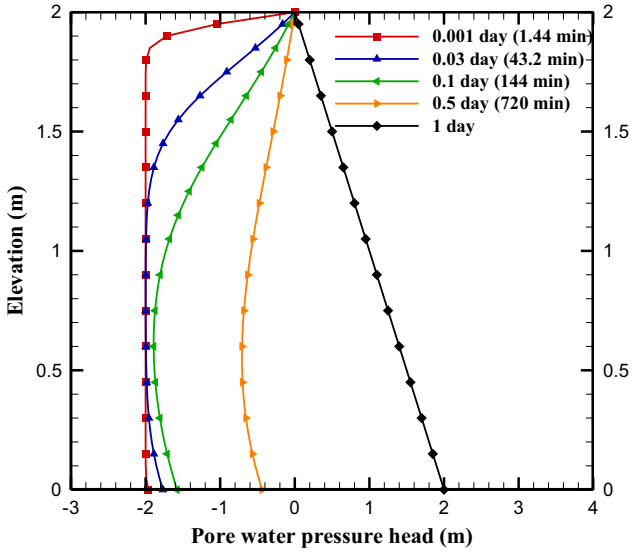

(a) Pore water pressure head profiles

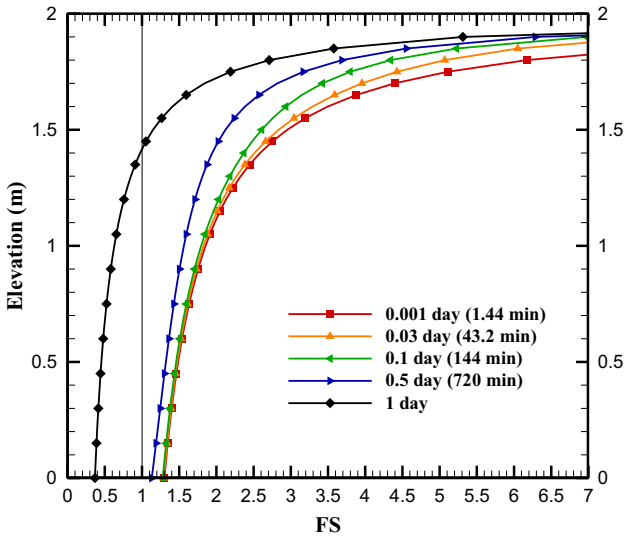

(b) Factor of safety profiles

Fig. 2. Results of deterministic analysis with propagation of rainfall infiltration.

the factor of safety at each potential slip surface. This destabilizing effect makes the minimum value of factor of safety of this slope decrease below 1.

This deterministic analysis provides a basic understanding of propagation of the flow field and the evolution of stability at different portions within the slope during the rainfall infiltration process, which helps to further investigate the effect of uncertainty or spatial variability of soil properties on the uncertainty in slope stability analysis.

3.2. Homogeneous slope

Here, we use a homogeneous slope model to investigate the effect of uncertainty of soil properties on the uncertainty of slope stability over time. Again, the uncertainty represents the unknown values of the homogeneous soil properties due to lack of measurements or errors in the measurements. The temporal evolutions of the cross correlation between the soil properties, including hydraulic property K_s and mechanical properties c', $\tan\phi'$, of the homogeneous slope and the FS_i at selected potential slip surfaces ($i = 39, 30, 20, 2$, i.e., $z_i = 1.9, 1.45, 0.95, 0.1$ m) are illustrated in Fig. 3. Besides the cross correlations, we also plot the σ^s with time corresponding to each observed potential slip surface. Note that the coefficient of variations (COVs, defined as σ/μ where σ denotes the standard deviation and μ denotes the mean) of all the parameters are set to 1.

As illustrated in Fig. 3, FS_i at an observed potential slip surface is negatively correlated with K_s. Physically, this means that if the FS_i evaluated at the observed potential slip surface is high, or in other words, the potential slip surface appears stable and reliable, the K_s value of this slope is likely low and vice versa. Because less flow is permitted to enter the slope with a K_s value smaller than its mean value, the pore-water pressure in the slope will not increase rapidly as the one simulated with the mean value. As a result, the slope stability becomes higher than the one under the infiltration in a slope with the mean K_s value.

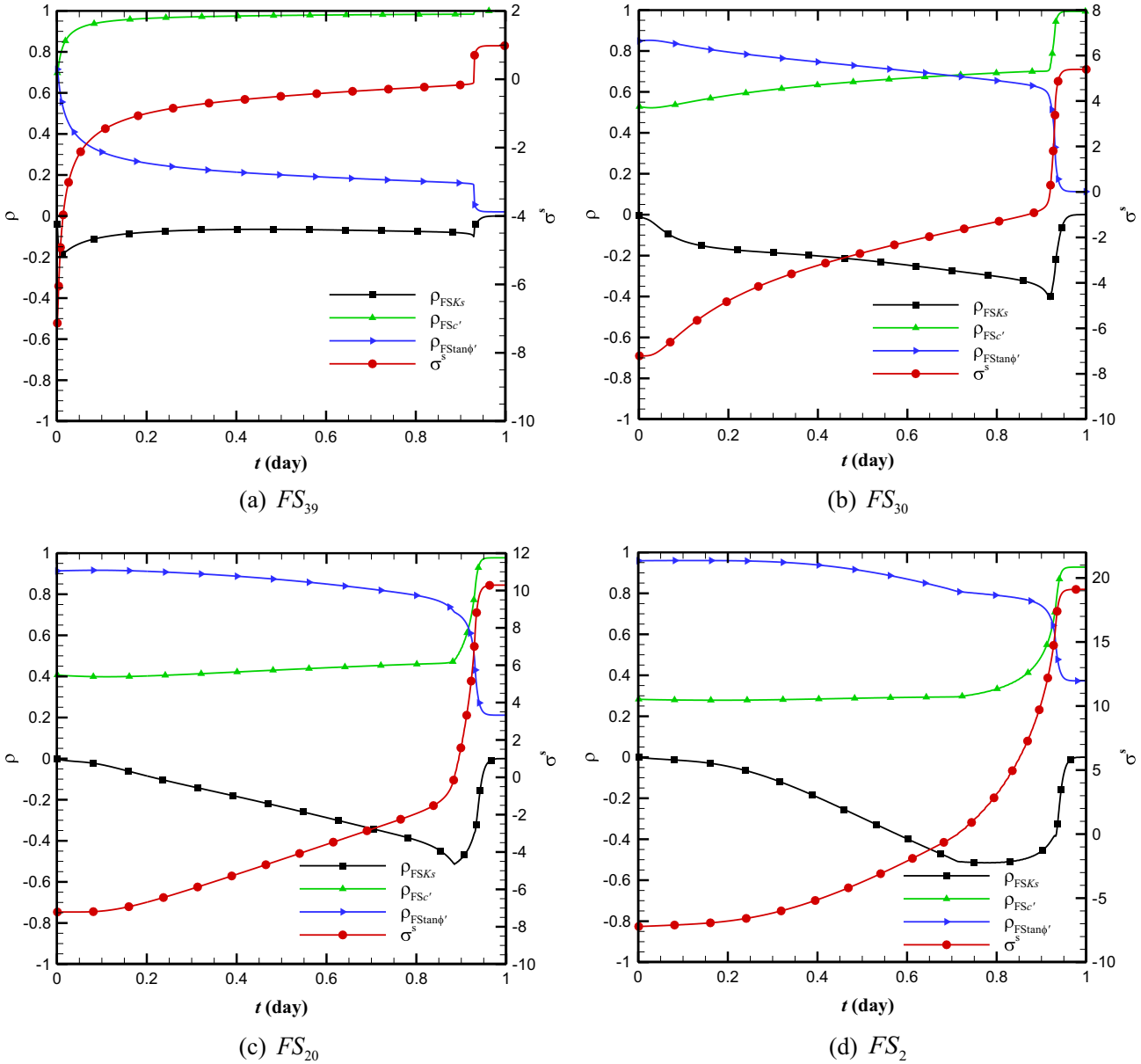

Fig. 3. Cross correlation as a function of t between K_s, c', $\tan\phi'$ of homogeneous slope and FS_i at observed potential slip surfaces ($i = 39, 30, 20, 2$, $z_i = 1.9, 1.45, 0.95, 0.1$ m), associated with σ^s as a function of t.

In Fig. 3, FS_i at an observed potential slip surface is positively correlated with c' and $\tan\phi'$. These results are expected because a slope with higher values of c' and $\tan\phi'$ is more stable than that with lower values of c' and $\tan\phi'$.

Generally speaking, the temporal evolutions of the cross correlation between the FS_i at different selected potential slip surfaces with the parameters are similar. On one hand, the cross correlation between FS_i and c' (i.e., $\rho_{FS_ic'}$, the green line with deltas in Fig. 3) increases with the elevation. On the other hand, the cross correlation between FS_i and $\tan\phi'$ (i.e., $\rho_{FS_i\tan\phi'}$, the blue line with right triangles in Fig. 3) decreases with the elevation. These results imply that ϕ' becomes more critical to slope stability than c' with the increase of normal stress and vice versa. The variation of the cross correlation between FS_i and K_s (i.e., $\rho_{FS_iK_s}$ denoted as the black line with squares in Fig. 3) as a function of time at the higher elevation (e.g., FS_{39}) is smaller but sharper than that at the lower elevation (e.g., FS_2). Note that $\rho_{FS_iK_s}$, $\rho_{FS_i\tan\phi'}$ and $\rho_{FS_ic'}$ all vary over time with the flow or σ^s. $\rho_{FS_i\tan\phi'}$ decreases significantly due to increase of σ^s, while $\rho_{FS_ic'}$ keeps increasing and gradually becomes relatively higher than $\rho_{FS_i\tan\phi'}$. This finding demonstrates the important role of c' on stabilizing the slope under the influence of rainfall infiltration.At later times ($t > 0.9$ day), $\rho_{FS_iK_s}$ tends to zero. This stems from the fact that after the wetting front zone reaches the impermeable slope base, positive pore water pressure builds up, the phreatic surface in the slope rises to the land surface, the flow becomes statics (no flow) and the distribution of water pressure becomes hydrostatic.

3.3. Heterogeneous slope

As a well-known fact, geologic media are inherently heterogeneous at a multiplicity of scales. A heterogeneous slope model, which is more realistic than the homogeneous model, is used next to investigate the effect of spatial variability of different soil properties at different locations on the uncertainty of slope stability during rainfall infiltration process.

3.3.1. Sensitivity analysis

Fig. 4 shows the spatial distributions of the sensitivities of FS_{30} (at elevation $z = 1.45$ m) to each one of the parameters (K_s, c' and $\tan\phi'$) at every element along the profile at some selected times. Note all the sensitivities are evaluated at mean values of parameters. The corresponding distributions of pore water pressure and distributions of factor of safety at the selected times have been displayed in Fig. 2.As shown in Fig. 4a, the spatial distribution of sensitivity between FS_{30} and K_s ($J_{FS_{30}K_s}$) varies temporally and spatially until $t = 1$ day. We will denote the portion between the land surface and observed potential slip surface as the upstream portion, and the portion between the observed potential slip surface and slope base as the downstream portion. At early times (e.g., 0–0.03 day), the flow due to rainfall infiltration is mainly confined in the upstream portion. Therefore, an increase of K_s's at this upstream portion will increase the amount of water flowing to the observed potential slip surface, and reduce the value of FS_{30}. Thus the sensitivity between FS_{30} and K_s's in the upstream portion is negative. On the other hand, the perturbations of K_s's of downstream portion have no influence on FS_{30}, and hence the sensitivity between them is zero. As the infiltration process continues, the sensitivity between FS_{30} and K_s's in the upstream portion becomes more negative. As water infiltrates into the downstream portion, a decrease of K_s's at this downstream portion will reduce the drai-

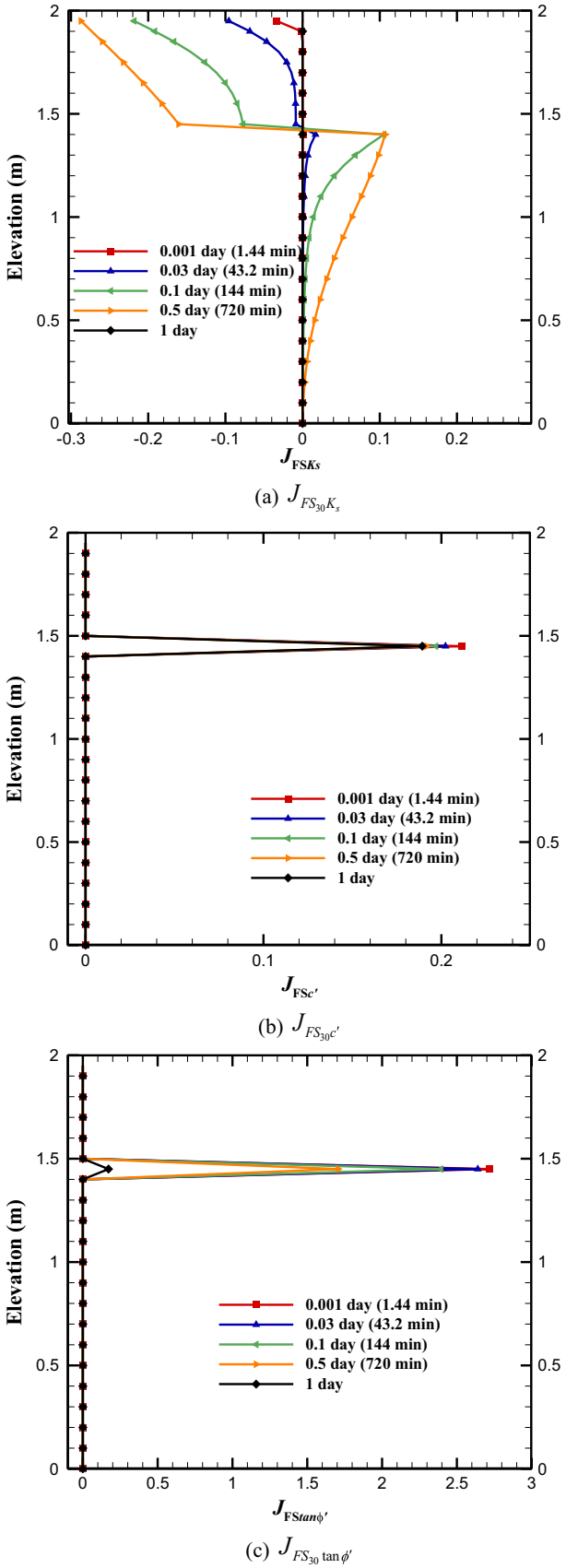

Fig. 4. Spatial distribution of sensitivity between FS_{30} and K_s, c', $\tan\phi'$ at different t.

nage of water from the observed potential slip surface, and decrease the value of FS_{30}. This explains the positive value of sensitivity between FS_{30} and K_s's in the downstream portion. Notice that perturbations of K_s at the location of FS_{30} have no influence on the FS_{30}. Overall, starting from the observed potential slip surface where FS_{30} is evaluated, the absolute value of $J_{FS_{30}K_s}$ increases along the upstream direction and decreases along the downstream direction. As explained in Section 3.2, at late times ($t > 0.9$ day), the distribution of water pressure becomes hydrostatic, $J_{FS_{30}K_s}$ becomes zero. That is, under this circumstance, perturbations of K_s's within the entire slope have no influences on the slope stability.As illustrated in Fig. 4b and c, only the perturbation of c' or $\tan\phi'$ at the potential slip surface where FS_{30} is evaluated can influence the FS_{30}. This result may be restricted to the limit equilibrium model (LEM) employed in this study, which does not consider deformation of the slope. In addition, sensitivities between FS_{30} and the mechanical parameters (i.e., c' and $\tan\phi'$) are positive. $J_{FS_{30}c'}$ can be viewed as temporal invariant because the influence of changes in unit weight (i.e.,γ_i) on the $J_{FS_{30}c'}$ is small. On the other hand, $J_{FS_{30}\tan\phi'}$ keeps decreasing during the infiltration. The values of $J_{FS_{30}c'}$ and $J_{FS_{30}\tan\phi'}$ are larger than the value of $J_{FS_{30}K_s}$ during almost all times of the infiltration.

3.3.2. Cross-correlation analysis

While cross-correlation analysis is similar to sensitivity analysis, it considers the effects of different magnitudes of heterogeneity (variance) of different parameters and the geological structure of the slope (correlation scales) (see Mao et al. [25] and Sun et al. [31]). Therefore, the cross-correlation analysis is deemed most appropriate to evaluate the relative impact of spatial variability of K_s, c' and $\tan\phi'$ on slope stability.The spatial distributions of the cross correlations between FS_{30} of the potential slip surface at elevation $z = 1.45$ m and each one of the parameters (K_s, c' and $\tan\phi'$), denoted as $\rho_{FS_{30}K_s}$, $\rho_{FS_{30}c'}$ and $\rho_{FS_{30}\tan\phi'}$, respectively, at some selected times are plotted in Fig. 5a, b and c. The COVs of the parameters are 1.0 and the correlation scale λ is 0.3 m.

As shown in Fig. 5a, generally, FS_{30} is negatively correlated with the K_s's in the upstream portion (i.e., from the land surface to the slip surface), and positively correlated with the K_s's in the downstream portion (i.e., below the slip surface). Because the flow is mainly confined in the upstream portion at early times (e.g., 0–0.03 day), the negative correlations between K_s's in the upstream portion and FS_{30} increases while the correlation between FS_{30} and K_s's in the downstream portion remains zero. As infiltration continues into intermediate times, the correlation between K_s's in the downstream portion and FS_{30} gradually increases from zero and becomes positive. Meanwhile, the cross correlation between FS_{30} and K_s's at the upstream portion continues to become more negative. As a result, a zero cross correlation point exists at around $z = 1.3$ m, and is under the observed potential slip surface ($z_{30} = 1.45$ m). Here we name this location as "reference point". Generally, starting from this reference point to either upstream or downstream, the absolute values of both positive and negative cross correlations first increase to a maximum, and then decreases as the distance increases.

FS_{30} has the maximum correlation with the c' or $\tan\phi'$ at the location (elevation $z = 1.45$ m) where FS_{30} is evaluated, and its correlation decreases gradually with the parameters at distances away $z = 1.45$ m due to the spatial correlation of the parameters (Fig. 5b and c). These figures also show that as infiltration continues, $\rho_{FS_{30}\tan\phi'}$ keeps on decreasing and $\rho_{FS_{30}c'}$ continues to increase.

Next, we illustrate the influence of correlation scale λ on the results of the cross-correlation analysis. The value of λ is changed from 0.3 m to 0.8 m. The resultant cross correlations between FS_{30} and each one of the parameters (K_s, c' and $\tan\phi'$) are shown in Fig. 5d, e, f, respectively.

As shown in Fig. 5d, at early times(e.g., 0–0.03 day), due to a larger value of λ, the negatively correlated portion at upstream expands doward in comparison with that in Fig. 5a. At intermediate times, the location of the reference point (i.e., the location with $\rho_{FS_{30}K_s}$ equals to zero) changes with time. By comparing Fig. 5d with Fig. 5a, it is found that when λ increases, the elevation of the reference point becomes much lower. These results all indicate that with a large λ, the autocorrelation between K_s at any two locations increases. The negative cross correlation, which has the absolute value larger than that of positive cross correlation, gradually becomes dominant within the slope. In addition, the distance between the location with the maximum negative cross correlation value and the reference point increases with λ.

In Fig. 5e and f, the temporal and spatial distributions of $\rho_{FS_{30}c'}$ and $\rho_{FS_{30}\tan\phi'}$ are similar to those in Fig. 5b, and c. As locations of parameters are away from the given potential slip surface ($z = 1.45$ m), $\rho_{FS_{30}c'}$ and $\rho_{FS_{30}\tan\phi'}$ decrease. Comparisons of Fig. 5b and c with Figs. 5e and f reveal that the spatial reduction rate of $\rho_{FS_{30}c'}$ and $\rho_{FS_{30}\tan\phi'}$ becomes smaller with the increase of λ. These results demonstrate that the cross correlation is not just sensitivity but it also includes our prior information of spatial structure of the property of the slope.

These aforementioned results imply that the stability of a potential slip surface is not equally influenced by parameters at all locations within the slope, and the influences from parameters at different locations on the stability of a potential slip surface change with time.

3.3.3. Uncertainties from each soil property

Next, we show in Fig. 6a, b, c and d the temporal evolution of standard deviation of FS_i, σ_{FS_i}, at four potential slip surfaces ($i = 39, 30, 20, 2$, i.e., $z_i = 1.9, 1.45, 0.95, 0.1$ m) of the slope due to the spatial variability of all parameters (K_s, c' and $\tan\phi'$). We also illustrate the contribution to σ_{FS_i} from the variability of each parameter. The correlation scale λ is 0.3 m. The COVs of the parameters are intentionally set to the same, 1.0.

According to these figures, the values of σ_{FS_i} (denoted as black solid lines in Fig. 6) at all four potential slip surfaces generally decrease with time. This reduction can be attributed to the fact that the influences of $\tan\phi'$ on FS_i decrease as the rainfall infiltrates the slope. In addition, the value of σ_{FS_i} at higher elevation is larger than that at lower elevation. This results stem from the fact that the contributions to σ_{FS_i} from variation of c' (denoted as green lines with deltas in Fig. 6) and $\tan\phi'$ (denoted as blue lines with circles in Fig. 6) increase with the elevation. The contribution to σ_{FS_i} from variation of c' keeps steady while the contribution to σ_{FS_i} from variation of $\tan\phi'$ decreases over the entire infiltration period. The impacts of the variations in K_s on FS_i (denoted as red lines with squares in Fig. 6) at 30th, 20th, and second potential slip surfaces continue to increase with the infiltration, except that at the 39th potential slip surface at the upper portion of slope, where the effect of variation in K_s on FS_i first increases sharply, then decreases with time. This phenomenon may be because that the 39th potential slip surface is close to the upper boundary so that the effect of variation in K_s on FS_{39} yields to the influence of the constant head boundary condition ($h = 0$) and eases with time. The impacts of the variations in K_s on FS_i at all four potential slip surfaces become zero at late time when the distribution of water pressure becomes hydrostatic. Overall, variations in c' and $\tan\phi'$ are shown to have greater effects on the FS_i than that of K_s.

However, in field sites, each soil property has its own degree of variation. To be more realistic, the typical range of COVs of param-

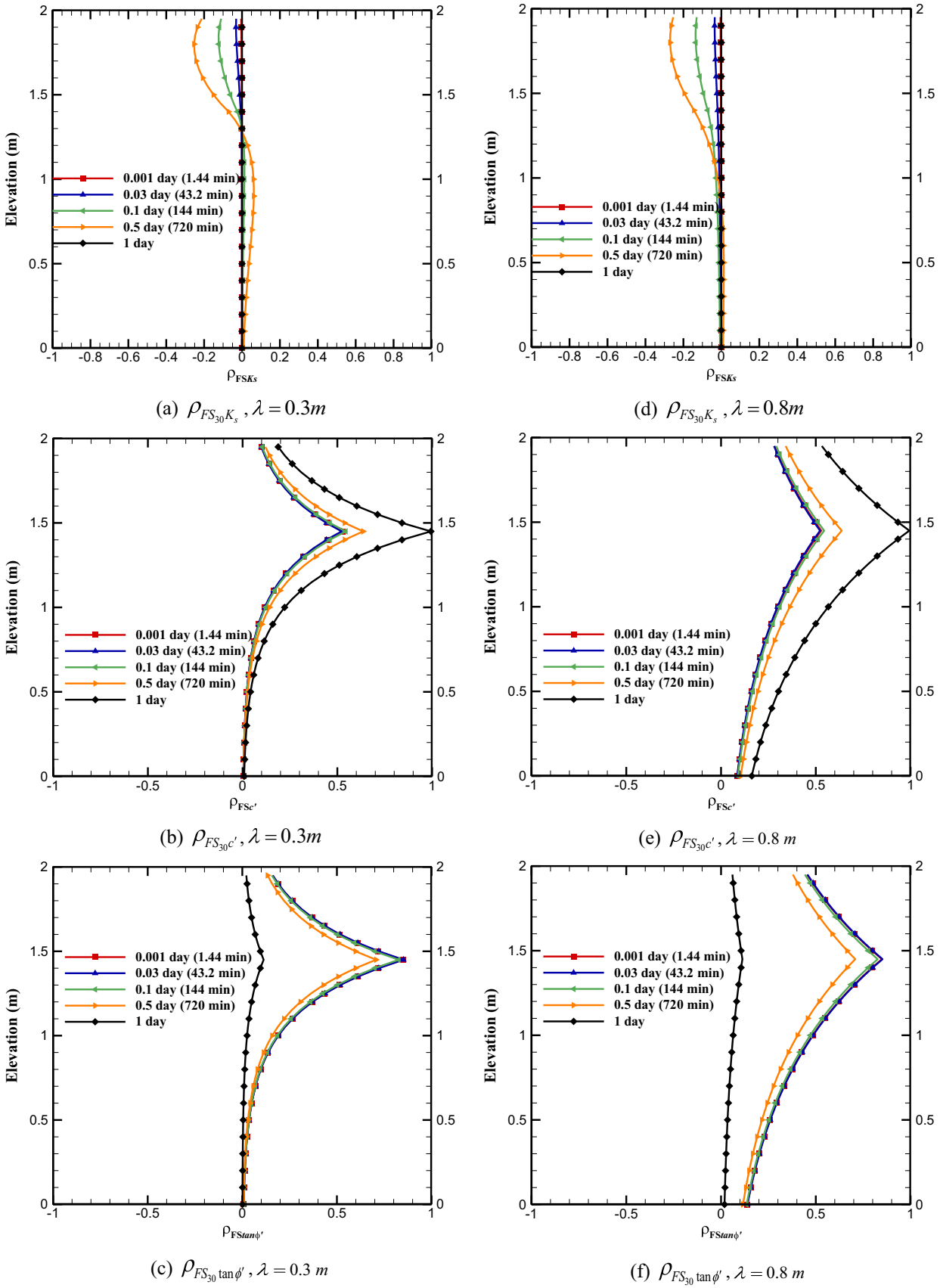

(a) $\rho_{FS_{30}K_s}, \lambda = 0.3m$ (d) $\rho_{FS_{30}K_s}, \lambda = 0.8m$

(b) $\rho_{FS_{30}c'}, \lambda = 0.3m$ (e) $\rho_{FS_{30}c'}, \lambda = 0.8\ m$

(c) $\rho_{FS_{30}\tan\phi'}, \lambda = 0.3\ m$ (f) $\rho_{FS_{30}\tan\phi'}, \lambda = 0.8\ m$

Fig. 5. Spatial distribution of cross correlation between FS_{30} and K_s, c', $\tan\phi'$ at different t with $\lambda = 0.3$ m (a, b, c) and $\lambda = 0.8$ m (d, e, f).

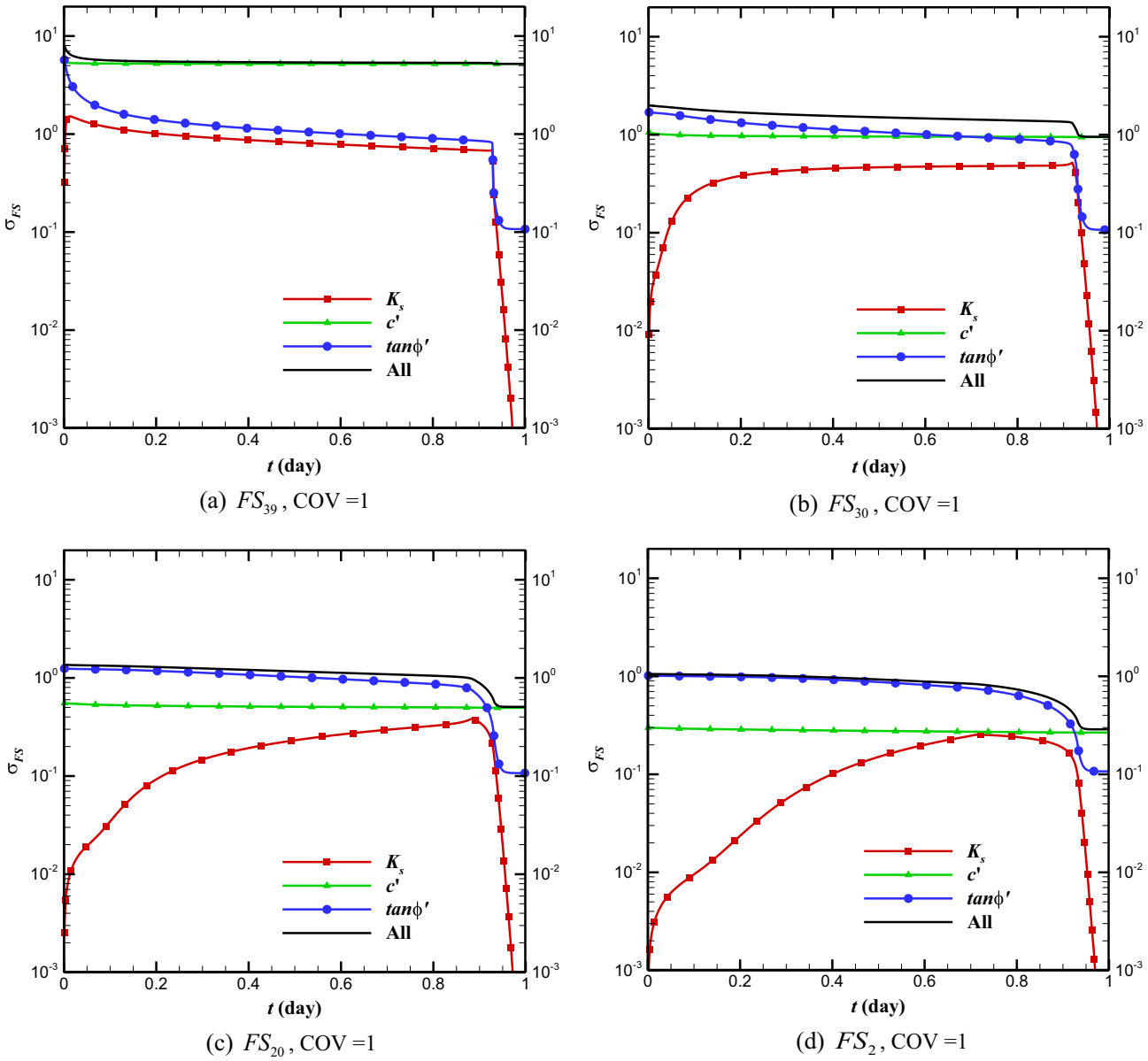

Fig. 6. Standard deviation of FS_i, σ_{FS_i}, for every parameter as a function of time with $\lambda = 0.3$ m and COVs of 1.

eters in the field should be taken into consideration. These typical ranges of COVs of these soil properties (K_s, c' and $\tan\phi'$) are obtained from available literature (e.g., [6,30]) and they are tabulated in Table 2. As shown in Table 2, the COV of K_s is much larger than those of c' and $\tan\phi'$. The lower bound of the range of COV of K_s is 27%. This is 4–7 times the lower bound of the range of COVs of c' and $\tan\phi'$, which are 4% and 6%, respectively. The upper bound of the range of COV of K_s reaches 767%, which is 10–20 times the upper bound of the range of COVs of c' and $\tan\phi'$.

Thereafter, we set the COVs of these parameters to the values of their own lower bound and upper bound, respectively. The similar plots for the temporal evolution of σ_{FS_i} are illustrated in Fig. 7a, b, c, and d for lower bound case and Fig. 7e, f, g, h for upper bound case. As expected, in both the lower bound case and the upper bound case, the contribution to σ_{FS_i} from variation in K_s is the most profound, and it persists over time before the flow reaches the hydrostatic condition. Influenced by variation in K_s, the values of σ_{FS_i} at 30th, 20th, second potential slip surfaces increase with time, and that at 39th potential slip surface mainly decreases with time, as explained previously. Comparisons of

Table 2
Typical ranges of COVs of soil properties (K_s, c' and $\tan\phi'$) base on Cao et al. [6] and Srivastava et al. [30].

Property	COV(%)
Ks	27–767
c'	4–84
$\tan\phi'$	6–46

Fig. 7a, b, c, and d with Fig. 7e, f, g, and h indicate that the temporal evolution of σ_{FS_i} at the same observed potential slip surface due to the variability of each parameter follows similar patterns, which have been illustrated in Fig. 6 and discussed previously. In addition, the values of σ_{FS_i} and the contribution to σ_{FS_i} from variation of each parameter in the upper bound case (Fig. 7e, f, g, and h) are larger than those in the corresponding ones with same observed potential slip surfaces in the lower bound case (Fig. 7a, b, c, and d). Such differences are attributed to the larger spatial variations in parameters in the upper bound case.

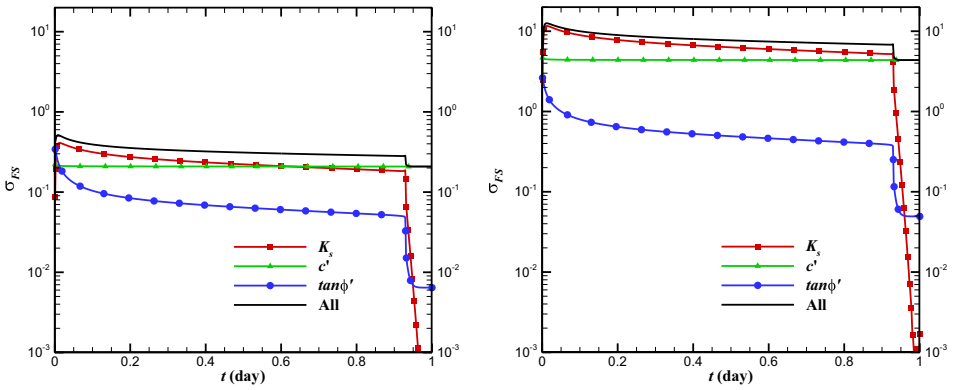

(a) FS_{39}, COV = lower bound

(e) FS_{39}, COV = upper bound

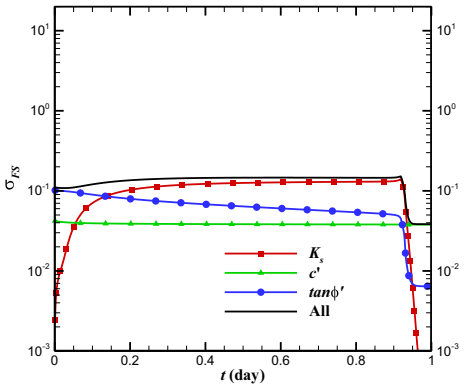

(b) FS_{30}, COV = lower bound

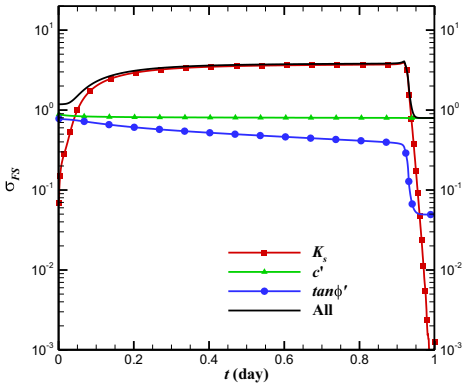

(f) FS_{30}, COV = upper bound

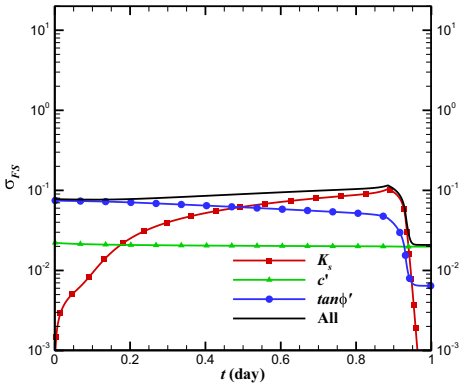

(c) FS_{20}, COV = lower bound

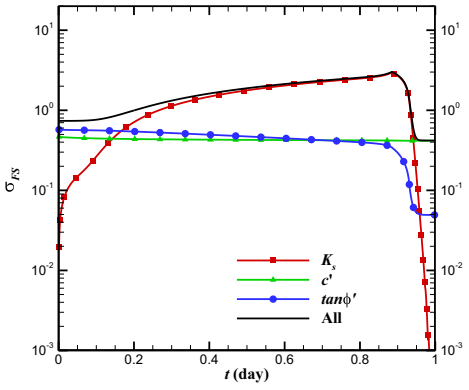

(g) FS_{20}, COV = upper bound

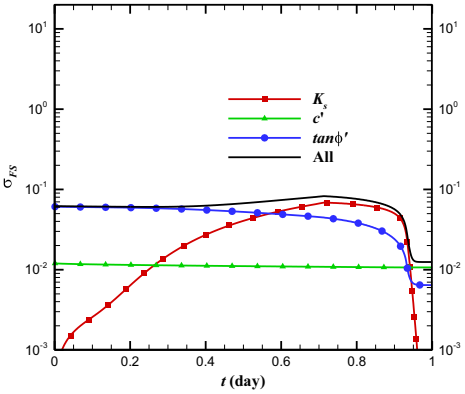

(d) FS_2, COV = lower bound

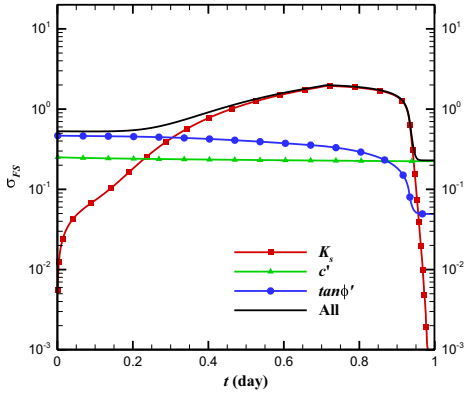

(h) FS_2, COV = upper bound

Fig. 7. Standard deviation of FS_i, σ_{FS_i}, for every parameter as a function of time with $\lambda = 0.3$ m and COVs equal to the lower bound (a, b, c, d) and the upper bound (e, f, g, h) of typical ranges, respectively.

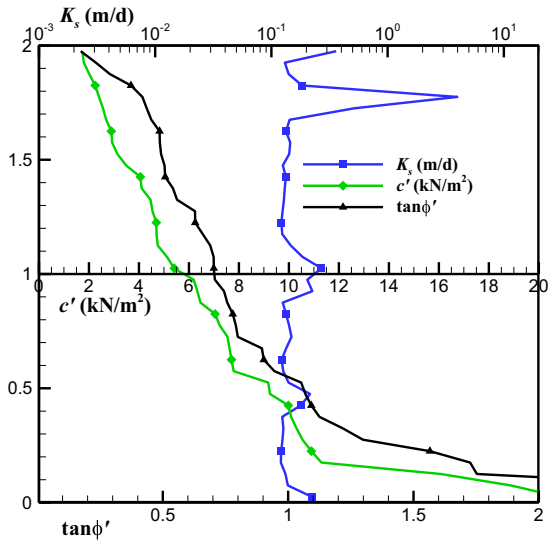

(a) K_s, c' and $\tan\phi'$ profile of Example 1

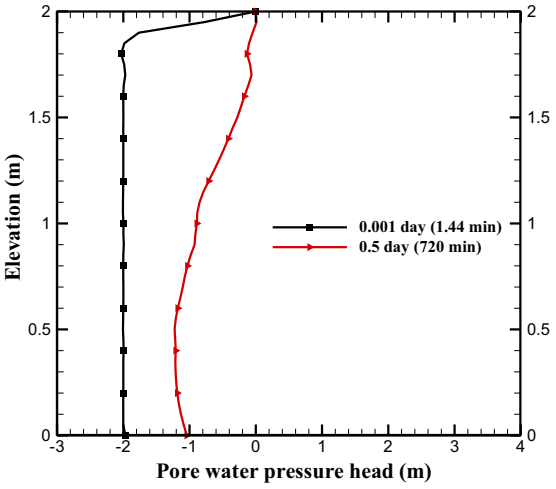

(b) Pore water pressure profile of Example 1

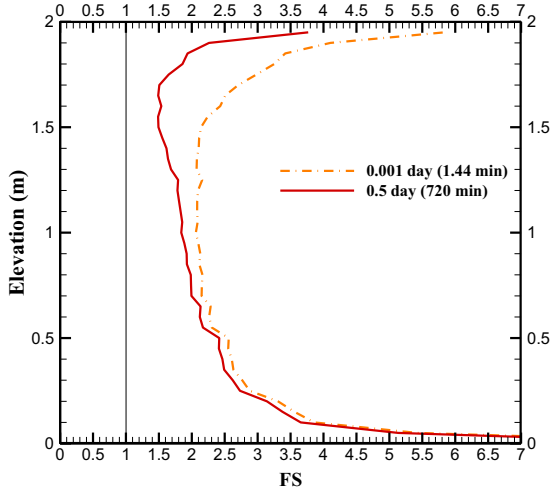

(c) FS_i profile of Example 1

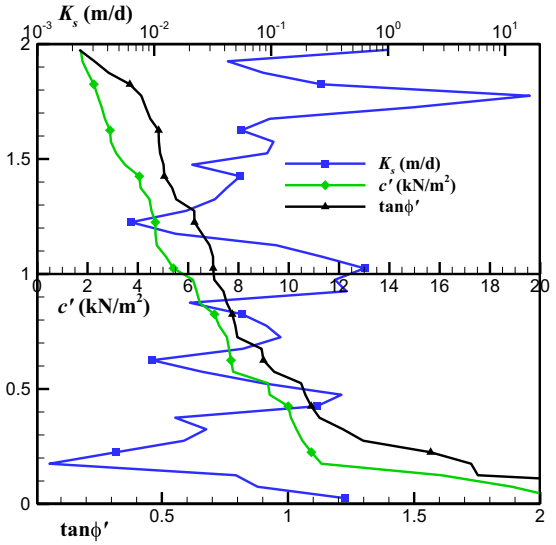

(d) K_s, c' and $\tan\phi'$ profile of Example 2

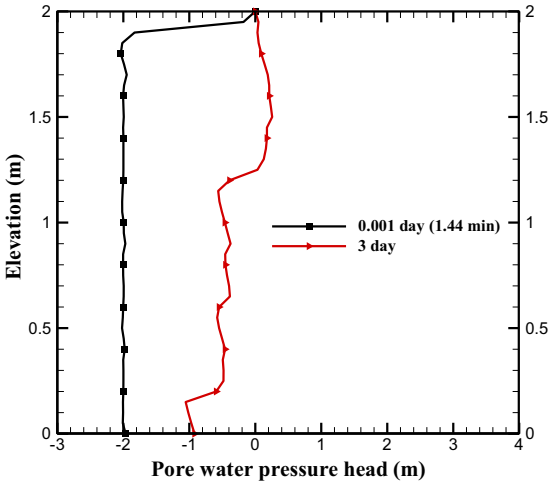

(e) Pore water pressure profile of Example 2

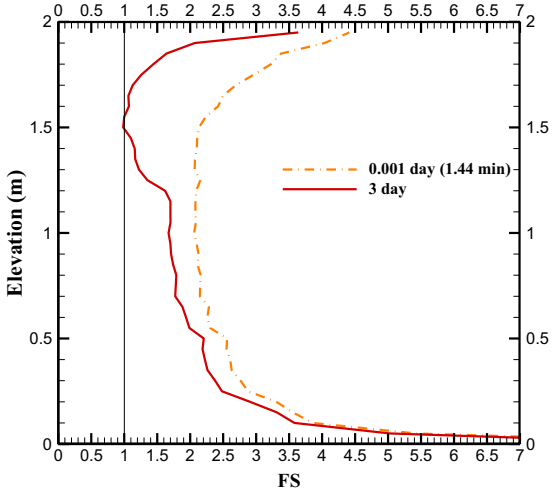

(f) FS_i profile of Example 2

Fig. 8. Typical realizations of the random field and the corresponding analysis results.

4. Application to typical realizations

For the purpose of demonstrating the importance of cross-correlation analysis on slope stability analysis, we examine two synthetic heterogeneous slopes (examples 1 and 2) under rainfall infiltration, and we then discuss their results of seepage and stability analysis. The profiles of K_s, c' and $\tan\phi'$ are shown in Fig. 8a and d for example 1 and example 2, respectively. As illustrated in the figures, the profiles of c' and $\tan\phi'$ are the same in these two examples, with the COVs equal to their upper bounds of typical ranges (i.e., 0.84 and 0.46, for c' and $\tan\phi'$, respectively). In addition, these realizations of c' and $\tan\phi'$ include linearly increasing mean trends with depth, as reported by Li et al. [22]. The difference between these two examples lies in the COV of K_s. Specifically, the realization of K_s in Example 1 is generated with COV = 1, while that in Example 2 is generated with COV equals to the upper bound of typical range of K_s (i.e., 7.67). That is, while the spatial patterns of K_s are the same, the heterogeneity of K_s in Example 1 is much smaller than that in Example 2. The correlation scale λ is 0.3 m for all these parameters (i.e., K_s, c' and $\tan\phi'$). The other related parameters remain the same as those in Table 1. We employ the Karhumen-Loève (K-L) expansion to generate these soil properties (K_s, c' and $\tan\phi'$), assuming they are log-normally distributed (e.g., [2,11,16,19,22,26–28]). Readers interested in K-L expansion are referred to other publications (e.g., [13,19,24]).

To simulate the rainfall infiltration process, the initial pressure head is assumed to be −2 m along the profile; the top boundary is set to 0 m, representing rainfall, and the bottom boundary condition is assumed impermeable. Based on cross correlation results shown in Fig. 5a, we choose a time when the rainfall infiltrates the slope to a certain depth and the effect of variation in K_s on slope stability is not zero. This selection allows examination of the effect of K_s's at most parts of the elevations of the slope. Hence, to reach the similar distribution of pore water pressure head within the slope (shown in Fig. 8b and e), Example 1 takes 0.5 day while Example 2 takes 3 days. This is due to the difference in the profile of K_s (solid blue lines with squares in Fig. 8a and d). The FS_i profiles at 0.001 s day and 0.5 days for the two examples are displayed in Fig. 8c and f. In both examples, at the very beginning of the rainfall infiltration, the spatial variation in FS_i profiles at 0.001 day (see the orange dash-dotted line in Fig. 8c and f) are mainly influenced by the spatial heterogeneity of c' and $\tan\phi'$ (see the green solid line with diamonds and the black solid line with deltas, respectively in Fig. 8a and d). They have little relationship with the spatial heterogeneity of K_s (the blue line with squares in Fig. 8a and d). Based on this result, the FS_i profile at 0.001 day will be used as a reference to determine whether the FS_i profiles at later times are influenced by the spatial heterogeneity of K_s.

In Example 1, as shown in Fig. 8c, the spatial variation of FS_i profile at 0.5 day (solid red lines) is not much different from that at 0.001 day (dash-dotted orange line). This implies the effect of heterogeneity of K_s on the spatial variation of FS_i profile remains insignificant, comparing to the spatial heterogeneity of c' and $\tan\phi'$. Although the COV of K_s (which is 1) is larger than those of c' and $\tan\phi'$ (which are 0.84 and 0.46, respectively), the impact of the spatial heterogeneity of K_s can be ignored. In other words, K_s can be simply treated as a spatial invariant parameter (e.g., the mean value of K_s) in the analysis of slope stability in this type of slopes under rainfall infiltration.

However, in Example 2 (COV of K_s = 7.67), the spatial heterogeneity of K_s has significant impacts on the spatial variation of FS_i profile at 3 days, as revealed by comparing the FS_i profile at 3 days (solid red line) with that at 0.001 day (dash-dotted orange line) in Fig. 8f. Notice that the FS_i at elevation of around 1.5 m along the FS_i profile becomes less than 1, which is the minimum of all FS_i ($i = 1, \ldots, n$), and it becomes the FS of the entire slope. Similarly, note that the K_s at upstream of this location is large, and the K_s at downstream is extremely small. The water pressure at this location is also highest as shown in Fig. 8e. This is consistent with the cross-correlation analysis discussed previously. That is, the stability of a potential slip surface is negatively correlated with the K_s's in the upstream portion, and positively correlated with the K_s's in the downstream portion. Hence, FS_i at this potential slip surface becomes smaller.

In summary, mechanical parameters such as c' and $\tan\phi'$ are intrinsic strength properties of a geologic medium, which have direct effect on slope stability. Meanwhile, hydraulic parameters (e.g., K_s) are secondary properties, which take effect on slope stability via water pressure. In view of this, the spatial heterogeneities of c' and $\tan\phi'$ should have greater effect on slope stability than that of K_s (in terms of sensitivity). However, K_s affects the effective stress of the slope, and the COV of K_s in the field is generally much larger than those of c' and $\tan\phi'$, as supported by the typical ranges shown in Table 2. The spatial heterogeneity of K_s thus can lead to large variability of the effective stress, and ultimately results in failure of a slope.

5. Conclusions

Generally, the stability of a potential slip surface is not equally influenced by every parameter at all locations within the slope, and the influences from each parameter at different locations change with time. Identifying the dominant parameter and its location at different times, and understanding how the parameter at a location at different times correlates with the stability of critical slip surface is important for design a site characterization scheme.

During the process of rainfall infiltration, the stability of a potential slip surface is generally negatively correlated with the K_s in the upstream portion, and positively correlated with the K_s in the downstream portion. The stability is also positively correlated with c' and $\tan\phi'$. The relative importance of $\tan\varphi'$ and c' depends on the effective stress. Specifically, the effect of $\tan\phi'$ on slope stability becomes larger than that of c' with the increase of the depth but it decreases with the accumulation of pore water pressure. As a result, the effect of c' on the slope stability becomes critical under the influence of rainfall.

The sensitivity of the stability of a slip surface to variability of c' and $\tan\phi'$ is found to be larger than that of K_s. Its effects on uncertainty of slope stability however may be small since the COVs of c' and $\tan\phi'$ in the field are generally small. On the other hand, while the sensitivity of the slope stability to the variability of K_s is small, impacts of this variability on slope stability could be large under heavy rainfall events since it controls the pore water pressure distribution in the slope. Moreover, the COV of K_s in the field is generally much larger than those of c' and $\tan\phi'$. This large variability may exacerbate the variability of pore water pressure even under normal rainfall events. Therefore, characterizing the heterogeneity of hydraulic properties like K_s and monitoring pore-water pressure distribution are critical to the slope stability analysis. Cost-effective approaches for characterizing K_s as suggested by Cai et al. [4] and hydraulic tomography (see [33,34,37]) become necessary.

Acknowledgements

This work was supported by the China Scholarship Council (Grant No. 201406410032); the National Natural Science Foundation of China (Grant Nos. 41172282, 41672313, 51409029, and

51479014); the Strategic Environmental Research and Development Program (Grant No. ER-1365); the Environmental Security and Technology Certification Program (Grant No. ER201212); the National Science Foundation-Division of Earth Sciences (Grant No. 1014594). The second author also acknowledges the Outstanding Oversea Professorship award through Jilin University from Department of Education, China as well as the Global Expert award through Tianjin Normal University from the Thousand Talents Plan of Tianjin City.

References

[1] Ali A, Huang J, Lyamin AV, Sloan SW, Griffiths DV, Cassidy MJ, et al. Simplified quantitative risk assessment of rainfall-induced landslides modelled by infinite slopes. Eng Geol 2014;179:102–16. http://dx.doi.org/10.1016/j.enggeo.2014.06.024.

[2] Brejda JJ, Moorman TB, Smith JL, Karlen DL, Allan DL, Dao TH. Distribution and variability of surface soil properties at a regional scale. Soil Sci Soc Am J 2000;64:974. http://dx.doi.org/10.2136/sssaj2000.643974x.

[3] Cai J-S, Yan E-C, Yeh T-CJ, Zha Y-Y, Liang Y, Huang S-Y, et al. Effect of spatial variability of shear strength on reliability of infinite slopes using analytical approach. Comput Geotech 2017;81:77–86. http://dx.doi.org/10.1016/j.compgeo.2016.07.012.

[4] Cai J-S, Yan E-C, Yeh TJ, Zha Y-Y. Sampling schemes for hillslope hydrologic processes and stability analysis based on cross-correlation analysis. Hydrol Process 2016. http://dx.doi.org/10.1002/hyp.11101.

[5] Cai J, Yan E, Yeh TJ, Zha Y. Effects of heterogeneity distribution on hillslope stability during rainfalls. Water Sci Eng 2016. http://dx.doi.org/10.1016/j.wse.2016.06.004.

[6] Cao Z, Wang Y, Li D. Quantification of prior knowledge in geotechnical site characterization. Eng Geol 2016;203:107–16. http://dx.doi.org/10.1016/j.enggeo.2015.08.018.

[7] Cho SE. Probabilistic stability analysis of rainfall-induced landslides considering spatial variability of permeability. Eng Geol 2014;171:11–20. http://dx.doi.org/10.1016/j.enggeo.2013.12.015.

[8] Cho SE. Probabilistic assessment of slope stability that considers the spatial variability of soil properties. J Geotech Geoenviron Eng 2010;136:975–84. http://dx.doi.org/10.1061/(ASCE)GT.1943-5606.0000309.

[9] Cho SE. Effects of spatial variability of soil properties on slope stability. Eng Geol 2007;92:97–109. http://dx.doi.org/10.1016/j.enggeo.2007.03.006.

[10] Cho SE, Lee SR. Instability of unsaturated soil slopes due to infiltration. Comput Geotech 2001;28:185–208. http://dx.doi.org/10.1016/S0266-352X(00)00027-6.

[11] Fenton GA, Griffiths D V. Risk assessment in geotechnical engineering; 2008.

[12] Gardner WR. Some steady-state solutions of the unsaturated moisture flow equation with application to evaporation from a water table. Soil Sci 1958;85:228–32. http://dx.doi.org/10.1097/00010694-195804000-00006.

[13] Ghanem RG, Spanos PD. Stochastic finite elements: a spectral approach. Courier Corporation; 2003.

[14] Griffiths DV, Fenton Ga. Probabilistic slope stability analysis by finite elements. J Geotech Geoenviron Eng 2004;130:507–18. 10.1061/(ASCE)1090-0241(2004)130:5(507).

[15] Griffiths DV, Huang J, Fenton GA. Influence of spatial variability on slope reliability using 2-D random fields. J Geotech Geoenviron Eng 2009;135:1367–78. http://dx.doi.org/10.1061/(ASCE)GT.1943-5606.0000099.

[16] Griffiths DV, Huang J, Fenton Ga. Probabilistic infinite slope analysis. Comput Geotech 2011;38:577–84. http://dx.doi.org/10.1016/j.compgeo.2011.03.006.

[17] Gui S, Zhang R, Turner JP, Xue X. Probabilistic slope stability analysis with stochastic soil hydraulic conductivity. J Geotech Geoenviron Eng 2000;126:1–9. http://dx.doi.org/10.1061/(ASCE)1090-0241(2000)126:1(1).

[18] Ji J, Liao HJ, Low BK. Modeling 2-D spatial variation in slope reliability analysis using interpolated autocorrelations. Comput Geotech 2012;40:135–46. http://dx.doi.org/10.1016/j.compgeo.2011.11.002.

[19] Jiang S-H, Li D-Q, Cao Z-J, Zhou C-B, Phoon K-K. Efficient system reliability analysis of slope stability in spatially variable soils using monte carlo simulation. J Geotech Geoenviron Eng 2015;141:4014096. http://dx.doi.org/10.1061/(ASCE)GT.1943-5606.0001227.

[20] Jiang S-H, Li D-Q, Zhang L-M, Zhou C-B. Slope reliability analysis considering spatially variable shear strength parameters using a non-intrusive stochastic finite element method. Eng Geol 2014;168:120–8. http://dx.doi.org/10.1016/j.enggeo.2013.11.006.

[21] Li D-Q, Qi X-H, Cao Z-J, Tang X-S, Phoon K-K, Zhou C-B. Evaluating slope stability uncertainty using coupled Markov chain. Comput Geotech 2016;73:72–82. http://dx.doi.org/10.1016/j.compgeo.2015.11.021.

[22] Li D-Q, Qi X-H, Phoon K-K, Zhang L-M, Zhou C-B. Effect of spatially variable shear strength parameters with linearly increasing mean trend on reliability of infinite slopes. Struct Saf 2014;49:45–55. http://dx.doi.org/10.1016/j.strusafe.2013.08.005.

[23] Lu N, Godt J. Infinite slope stability under steady unsaturated seepage conditions. Water Resour Res 2008;44:n/a–a. http://dx.doi.org/10.1029/2008WR006976.

[24] Lu Z, Zhang D. Stochastic simulations for flow in nonstationary randomly heterogeneous porous media using a KL-based moment-equation approach. Multiscale Model Simul 2007;6:228–45. http://dx.doi.org/10.1137/060665282.

[25] Mao D, Yeh T-CJ, Wan L, Lee C-H, Hsu K-C, Wen J-C, et al. Cross-correlation analysis and information content of observed heads during pumping in unconfined aquifers. Water Resour Res 2013;49:713–31. http://dx.doi.org/10.1002/wrcr.20066.

[26] Parkin TB, Meisinger JJ, Starr JL, Chester ST, Robinson JA. Evaluation of statistical estimation methods for lognormally distributed variables. Soil Sci Soc Am J 1988;52:323. http://dx.doi.org/10.2136/sssaj1988.03615995005200020004x.

[27] Parkin TB, Robinson JA. Analysis of lognormal data. In: Adv soil sci. Springer; 1992. p. 193–235.

[28] Phoon K-K, Kulhawy FH. Characterization of geotechnical variability. Can Geotech J 1999;36:612–24. http://dx.doi.org/10.1139/t99-038.

[29] Santoso AM, Phoon KK, Quek ST. Effects of soil spatial variability on rainfall-induced landslides. Comput Struct, vol. 89. Elsevier Ltd; 2011. p. 893–900. http://dx.doi.org/10.1016/j.compstruc.2011.02.016.

[30] Srivastava A, Babu GLS, Haldar S. Influence of spatial variability of permeability property on steady state seepage flow and slope stability analysis. Eng Geol 2010;110:93–101. http://dx.doi.org/10.1016/j.enggeo.2009.11.006.

[31] Sun R, Yeh TJ, Mao D, Jin M, Lu W, Hao Y. A temporal sampling strategy for hydraulic tomography analysis. Water Resour Res 2013;49:3881–96. http://dx.doi.org/10.1002/wrcr.20337.

[32] Tsai T-L, Tsai P-Y, Yang P-J. Probabilistic modeling of rainfall-induced shallow landslide using a point-estimate method. Environ Earth Sci 2015;73:4109–17. http://dx.doi.org/10.1007/s12665-014-3696-5.

[33] Yeh T-C, Khaleel R, Carroll KC. Flow through heterogeneous geological media. Cambridge University Press; 2015.

[34] Yeh T-CJ, Liu S. Hydraulic tomography: development of a new aquifer test method. Water Resour Res 2000;36:2095–105. http://dx.doi.org/10.1029/2000WR900114.

[35] Yeh TJ, Srivastava R, Guzman A, Harter T. A numerical model for water flow and chemical transport in variably saturated porous media. Ground Water 1993;31:634–44. http://dx.doi.org/10.1111/j.1745-6584.1993.tb00597.x.

[36] Zhu H, Zhang LM, Zhang LL, Zhou CB. Two-dimensional probabilistic infiltration analysis with a spatially varying permeability function. Comput Geotech 2013;48:249–59. http://dx.doi.org/10.1016/j.compgeo.2012.07.010.

[37] Zhu J, Yeh T-CJ. Characterization of aquifer heterogeneity using transient hydraulic tomography. Water Resour Res 2005;41:2372–80. http://dx.doi.org/10.1029/2004WR003790.